

Aminofunctionalized silica monolith for Pb²⁺ removal: synthesis and adsorption experiments

Hakimeh Sharififard^{a,c}, Paolo Aprea^{b,*}, Domenico Caputo^b, Francesco Pepe^{c,*}

^aDepartment of Chemical Engineering, Amirkabir University of Technology, No.424, Hafez Ave., Tehran, Iran, email: hakimeh.sharifi@gmail.com

^bACLabs – Applied Chemistry Laboratories, Department of Chemical, Materials and Industrial Production Engineering, Università Federico II, P.le Tecchio 80, 80125, Napoli, Italy, email: paolo.aprea@unina.it (P. Aprea), domenico.caputo@unina.it (D. Caputo)

^cDepartment of Engineering, Università del Sannio, Piazza Roma 21, 82100 Benevento, Italy, email: francesco.pepe@unisannio.it

Received 15 February 2017; Accepted 31 January 2018

ABSTRACT

Lead(II) removal from aqueous solutions by adsorption on APTMS-functionalized silica monolith (APTMS-Monosil) was investigated. Functionalized silica monolith was selected as adsorbent due to its ease of synthesis and versatility. Adsorption experiments were performed in a batch system, and the effects of various operating parameters, such as solution pH, initial concentration and solid to liquid ratio were evaluated. According to the Response Surface Methodology results, the optimum operating conditions for Pb²⁺ removal by APTMS-Monosil were pH = 6.24, initial Pb²⁺ concentration of 89.5 mg L⁻¹ and solid to liquid ratio of 1.84 g·L⁻¹. The kinetic data suggested that chemical adsorption, rather than mass transfer, was the controlling step for lead capture. Equilibrium isotherms were analyzed using different models, and data were well fitted to the Langmuir isotherm. The thermodynamic parameters of the adsorption process ($\Delta H^\circ = 30.9 \text{ kJ}\cdot\text{mol}^{-1}$, $\Delta S^\circ = 0.187 \text{ kJ}\cdot\text{mol}^{-1} \text{ K}^{-1}$, and $\Delta G^\circ = -24.826 \text{ kJ}\cdot\text{mol}^{-1}$ at $T = 298 \text{ K}$), calculated from three isotherms at $T = 30\text{--}60^\circ\text{C}$, revealed a spontaneous, endothermic process, with a strong chemical nature. The maximum adsorption capacity of APTMS-Monosil for lead was 450 mg·g⁻¹, which is a high value if compared with other materials presented in the literature.

Keywords: Silica monolith; Amine functionalization; Lead adsorption; Response surface method

1. Introduction

Heavy metal contamination of water resources is one of the greatest environmental concerns because of the toxic effects that these substances have for human beings and other animals and plants in the environment, and because of their tendency to bioaccumulate. One of the most ubiquitous heavy metals is lead, that is released to environment through a number of industrial activities such as refineries, printing, production of pigments *etc.* [1–5]. The presence of lead in water, even at very low concentrations, is extremely harmful to the aquatic environment and human

health. Lead can damage, among others, the nervous system, kidney, and reproductive system [6]. The World Health Organization (WHO) and US Environmental Protection Agency (US EPA) have set a maximum guideline concentration of 0.01 and 0.015 mg·L⁻¹ for Pb in drinking water, respectively [7].

Several technologies, such as chemical precipitation, electrocoagulation, ion exchange, membrane processes and adsorption have been tested for heavy metal removal from industrial wastewater [8–17]. Among them, adsorption seems to be the most suitable method in case of low concentration of contaminant, due to its relatively low cost and high efficiency [18,19]. With the increase in global awareness for environmental pollution, there is a growing

*Corresponding author.

demand for novel adsorbents characterized by high performances and efficiency for removal of heavy metals from aqueous systems, and quite recently several adsorbents have been tested, such as metal oxides/hydroxides [20,21], zero valent iron composites [22,23], and surfactant modified materials [24,25].

Among the materials of interest for adsorption applications are ordered mesoporous silicas (OMS). OMS constitute a large class of mainly amorphous materials, whose greatest advantages are their relatively large, yet uniform pore size, large surface area, and easily controllable surface chemistry [26,27]. However, since OMS have no strong affinity towards heavy metals, it is necessary to modify them by insertion of appropriate functional groups, such as amino groups, in order to increase their adsorption performances [13,28–31].

OMS are typically synthesized as powders, and their textural properties are subject to degradation during aggregation/shaping processes. An interesting alternative to powder functionalization followed by aggregation is the use of substrates directly obtained as aggregate materials, such as macro/mesoporous silica monoliths that can be subjected to a post synthesis functionalization process [32]. Silica monoliths, which can be produced by different synthesis routes [32–34], feature high chemical and mechanical stability, and their surface can be readily functionalized via grafting of organic and inorganic moieties [35]. According to published literature, there are few research works regarding the application of silica monoliths for heavy metal removal. For example, Sugrue and coworkers [36] modified a commercially available chromatographic silica column with iminodiacetic acid, reporting some encouraging results about its ion-exchange properties. Awual and coworkers [37,38], on the contrary, performed a direct synthesis of silica monoliths followed by a direct immobilization of functional acids, in order to perform an efficient removal of copper and cobalt from aqueous solutions.

The goal of the present investigation is the evaluation of a silica monolith, named Monosil [35], functionalized with 3-aminopropyl-trimethoxysilane for the removal of Pb^{2+} ions from aqueous solutions. The effect of several operating parameters, such as initial pH, lead concentration and solid to liquid ratio on removal efficiency is investigated in batch conditions using Central Composite Method (CCD) with response surface methodology (RSM), and kinetic and equilibrium data are thoroughly analyzed in order to better clarify the lead adsorption mechanisms.

2. Materials and methods

2.1. Synthesis and characterization of APTMS-Monosil

Monosil silica monoliths were synthesized following the approach adopted in [35]. 23.15 g of deionized water and 2.3 g of HNO_3 (68%) were mixed for 15 min at 0°C. Afterwards, 2.4 g of polyethylene oxide (PEO, 20 kDa) was added, and the mixture was stirred for 1 h. After that, 18.9 g of tetra-ethyl-ortho-silicate (TEOS) was added, and the new mixture was further stirred for 1 h. The solution was then poured into plastic tubes of 10 cm length and 8 mm internal diameter, and was kept at 40°C for 24 h to allow

complete solidification. The monoliths, of cylindrical shape, were extracted from the tubes, washed in water, and then treated in an ammonia solution (0.1 M) at 40°C for 24 h. Finally, they were dried at 40°C overnight and calcined at 550°C for 8 h.

In order to perform adsorption experiments, the monoliths were crushed and sieved to select 2–3 mm particles. The selected particles were functionalized with 3-aminopropyl-trimethoxysilane (APTMS) using a wet impregnation method. Initially, they were dried at 100°C for 24 h; then, grafting of aminic groups was carried out by refluxing 0.1 g of Monosil in a 50 mL dry toluene solution containing 0.25 mL of 97% pure APTMS at 110°C for 24 h. The APTMS functionalized particles were then collected and washed with toluene, and then dried at room temperature for 24 h. All reagents for the synthesis procedure were purchased from Sigma Aldrich Co., while deionized water ($\sigma \leq 0.055$ mS/cm) was prepared in house.

The surface area (S_{BET}) and pore size distribution of both raw Monosil and APTMS-Monosil were determined from adsorption-desorption isotherms of N_2 at 77 K. A Quantachrome NOVA 1000 surface area analyzer was used to determine the isotherms. Furthermore, pH_{ZPC} (point of zero charge) of APTMS-Monosil was measured using the following technique: 0.3 g of adsorbent was added to 50 mL of a 0.1 N NaCl solution, the pH of which was adjusted using aqueous HCl or NaOH solutions. The pH_{ZPC} of the adsorbent was assumed to coincide with the initial solution pH if this remained constant after addition of the adsorbent and thorough mixing [15]. Fourier Transform Infrared (FT-IR) spectra of the samples were recorded between 4000 and 400 cm^{-1} using the KBr method, with a resolution of 4 cm^{-1} with a Nicolet FT-IR spectrophotometer (NEXUS 670).

2.2. Effect of adsorption parameters

The effects of three operating parameters, namely solution pH, solid to liquid ratio and initial concentration, were investigated. Batch Pb^{2+} adsorption experiments were performed by adding a measured weight of APTMS-Monosil in 50 mL of Pb^{2+} solutions with an assigned initial Pb^{2+} concentration and pH. Reagent grade $\text{Pb}(\text{NO}_3)_2$ from Sigma-Aldrich Co. and deionized water were used to prepare the solutions. The initial pH of the solutions was adjusted with HCl and NaOH solutions. The mixtures, kept in 100 mL Erlenmeyer flasks, were shaken at 30°C using an orbital shaker (FINEPCR-SH30) at 150 rpm for 3 h. At the end of the experiment, the adsorbent was separated from liquid phase by filtration on filter paper (Whatman No. 40). The residual Pb^{2+} concentration in solution was determined using Inductively Coupled Plasma Optical Emission Spectrometry (ICP OES, Perkin Elmer Optima 2100 DV), and the comparison between initial and final Pb^{2+} concentrations allowed to evaluate the removal percentage.

With the purpose of assessing the role of the three operating parameters mentioned above, CCD was used. Since the number of independent parameters is three, 20 experiments consisting of 8 factorial points, 6 axial points and 6 replicates at the center points were carried out [39–43]. The range of variables investigated is given in Table 1.

Table 1
Experimental ranges and levels of independent variables

Independent parameter	Actual form of coded levels		
	-1	0	+1
X_1 pH	2	4.35	6.7
X_2 Solid to liquid ratio	0.5	1.75	3
X_3 Initial Pb^{2+} concentration	10	55	100

2.3. Kinetic studies

The kinetics of adsorption were studied by placing 0.05 g of adsorbent in flasks containing 50 mL of $100 \text{ mg}\cdot\text{L}^{-1}$ Pb^{2+} solution at pH 6.0. The flasks were agitated in the orbital shaker at 150 rpm for a time ranging between 2–360 min at 30°C . After that, the suspension was filtered, and the solution concentration was analyzed. The metal uptake was calculated as:

$$q = \frac{V}{m}(C_0 - C_f) \quad (1)$$

where q is the amount of solute adsorbed per unit weight of adsorbent ($\text{mg}\cdot\text{g}^{-1}$), V and m are solution volume (L) and dry weight of adsorbent (g), respectively, and C_0 and C_f are the initial and final metal ion concentration ($\text{mg}\cdot\text{L}^{-1}$), respectively.

2.4. Equilibrium studies

The adsorption isotherms for Pb^{2+} on APTMS-Monosil were determined by placing 0.025 g of adsorbent in a series of flasks containing 50 mL of metal ion solutions at different initial concentrations (10 – $220 \text{ mg}\cdot\text{L}^{-1}$). Initial pH was adjusted at 6.0 in all experiments. The flasks were agitated in an orbital shaker at 150 rpm for 24 h at various temperatures (30° , 45°C and 60°C). After this period, the suspension was filtered and the residual Pb^{2+} concentration was determined. The amount of lead adsorbed, q , was calculated using Eq. (1).

2.5. Regeneration and reuse of APTMS-Monosil

The regeneration tests of APTMS-Monosil were carried out as follows: 0.05 g of adsorbent, previously saturated with Pb^{2+} ions by contacting it with a $100 \text{ mg}\cdot\text{L}^{-1}$ Pb^{2+} solution at pH 6.0 for 48 h, was treated with 5 ml of 0.1 M EDTA solution under vigorous stirring at 50°C for 1 h, followed by washing with deionized water for several times and drying at 80°C for 2 h. The regenerated adsorbent was then used for the next adsorption test. Five consecutive adsorption–regeneration cycles were performed to check the reusability of the APTMS-Monosil for capturing Pb^{2+} [44].

3. Results and discussion

3.1. Characterization of the adsorbents

The porosity parameters of Monosil and APTMS-Monosil are presented in Table 2. The surface area was calculated by applying the 3-point BET (Brunauer–Emmett–Teller) method. The volume ($\text{mL}\cdot\text{g}^{-1}$) of micropore and mesopore

Table 2
Porosity parameters of Monosil and APTMS-Monosil

Parameter	Monosil	APTMS-Monosil
BET Sp. Surf. area ($\text{m}^2\cdot\text{g}^{-1}$)	543	163
Mesopore volume ($\text{mL}\cdot\text{g}^{-1}$), BJH method	0.844	0.327
Micropore volume ($\text{mL}\cdot\text{g}^{-1}$), HK method	0.032	0.042
Average pore radius (\AA)	32.3	43.3

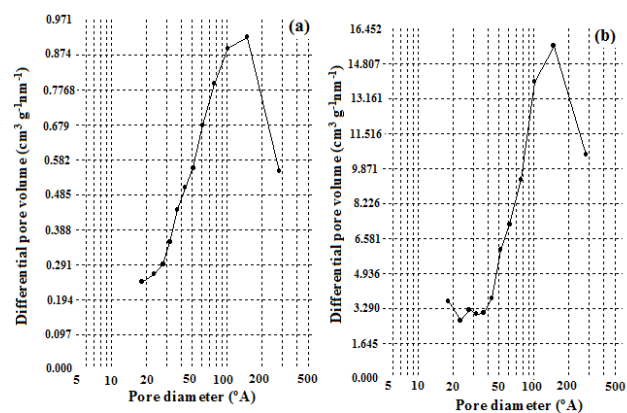


Fig. 1. BJH differential pore size distribution of: (a): Monosil, (b): APTMS-Monosil.

was determined by HK (Horvath–Kawazoe) and BJH (Barrett, Joyner, and Halenda) methods, respectively [45,46].

BJH differential pore size distribution (Fig. 1) shows that both Monosil and APTMS-Monosil have a mesoporous structure. It can be seen that functionalization of Monosil with APTMS causes a reduction in surface area and pore volume: this can be interpreted by assuming that the molecules of APTMS diffuse into the mesoporous structure of Monosil, limiting the accessibility of N_2 molecules to smaller pores. As a result, the average pore radius of the APTMS-Monosil is higher compared to that of Monosil. The pH_{ZPC} of APTMS-Monosil is 4.9.

The FT-IR spectra of Monosil and APTMS-Monosil are shown in Fig. 2. In both spectra, the two peaks located at around 3450 cm^{-1} and 1630 cm^{-1} can be attributed to the stretching and bending modes of adsorbed water molecules, while the peak at around 950 cm^{-1} is due to asymmetric vibrations of (Si–OH), thus revealing the presence of hydroxyl groups. The asymmetric, stretching and bending vibrations of (Si–O–Si) are responsible for the peaks at 1090 cm^{-1} , 800 cm^{-1} and 460 cm^{-1} , respectively [47]. After modification of Monosil with APTMS, new peaks are detected between 1610 cm^{-1} and 1715 cm^{-1} . These new peaks represent the vibration of different amine groups such as NH_2 [26].

3.2. Effect of separation parameters

3.2.1. Regression model equation development

The complete design matrix and the response values obtained from the experimental works are reported in

Table 3, together with a comparison with the prediction of Eq. (2). Eq. (2) represents the empirical quadratic model that was used to fit the experimental data, with the coefficients of this model obtained by multiple regression analysis technique using Design-Expert® 7.0 software:

$$\begin{aligned} \text{Removalpercentage} = & -95.56 + 53.59X_1 + 52.32X_2 - 0.45X_3 \\ & -5.69X_1X_2 + 7.44 \cdot 10^{-3}X_1X_3 + 7.77 \cdot 10^{-3}X_2X_3 \quad (2) \\ & -3.74X_1^2 - 4.26X_2^2 + 3.47 \cdot 10^{-3}X_3^2 \end{aligned}$$

As indicated in Table 1, in this equation X_1 , X_2 and X_3 are solution pH, solid to liquid ratio (g L^{-1}) and initial concentration of Pb^{2+} (mg L^{-1}), respectively.

The analysis of variance (ANOVA) was applied in order to critically evaluate the role played by the different variables considered. The ANOVA results are shown in Table 4. According to the rule, the best regression model is deter-

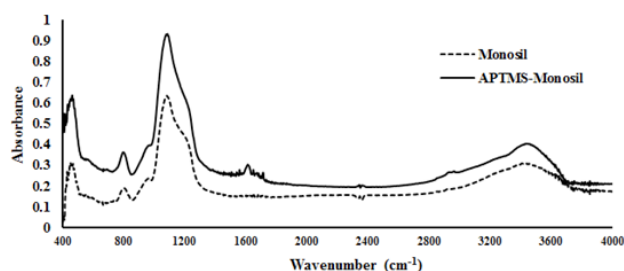


Fig. 2. FT-IR spectra of Monosil and APTMS-Monosil.

mined by highest Fisher's F values and lowest p -values [43,48]. Data in Table 4 indicate that the quadratic model was significant at the 90% confidence level. As it can be seen from inspection of Table 4, the F value for the model is 77.1, and correspondingly the p -value is lower than 0.0001 and SS is quite high ($SS = 1.81 \cdot 10^4$). This implies that the model is significant, and that it can appropriately explain the relationship between response and variables individuated as independent. This conclusion is also confirmed by the fact that both R^2 and R^2_{adj} approached unity. Furthermore, p -values that are lower than 0.05 allow to individuate the model terms which are significant, while values greater than 0.1 allow to individuate model terms are not significant, and can be omitted [49]. According to the results reported in the ANOVA table, the linear, quadratic and combined effects of pH (X_1) and solid to liquid ratio (X_2) are the most significant variables, while Pb^{2+} concentration plays a less relevant role, at least in the concentration range explored here.

The fact that Pb^{2+} concentration is practically irrelevant probably depends on the fact that the adsorbent is far from saturation. Eliminating the less significant terms from Eq. (2) and refining the model, Eq. (2) may be simplified to:

$$\begin{aligned} \text{Removalpercentage} = & -95.56 + 53.59X_1 + 52.32X_2 - 5.69X_1X_2 \\ & -3.74X_1^2 - 4.26X_2^2 \quad (3) \end{aligned}$$

A further confirmation of the validity of the analysis now presented comes from the diagnostic plot of Fig. 3, in which the values predicted by Eq. (3) are reported vs. experimental data, with a very satisfactory comparison.

The different roles played by the three independent variables under consideration are graphically described in

Table 3
Experimental conditions and results for lead removal

Run	pH	Solid to liquid ratio (g L^{-1})	Initial concentration (mg L^{-1})	Actual removal (%)	Predicted removal (Eq. (2), %)
1	1.49	1.75	55.00	30.1	27.42
2	4.35	1.75	55.00	89.9	90.26
3	4.35	1.75	55.00	90.4	90.26
4	2.00	3.00	10.00	76.1	77.23
5	7.21	1.75	55.00	83	92.57
6	6.70	0.50	10.00	100	98.30
7	4.35	3.27	55.00	96	97.31
8	4.35	1.75	55.00	92	90.26
9	6.70	0.50	100.00	100	96.72
10	6.70	3.00	10.00	100	96.44
11	4.35	1.75	55.00	92.6	90.26
12	2.00	0.50	10.00	11	12.10
13	4.35	1.75	0.28	100	101.88
14	2.00	0.50	100.00	6.1	7.65
15	4.35	0.23	55.00	58.5	60.53
16	6.70	3.00	100.00	100	96.88
17	2.00	3.00	100.00	74.7	74.66
18	4.35	1.75	55.00	91.6	90.26
19	4.35	1.75	109.72	95.2	99.43
20	4.35	1.75	55.00	93.6	90.26

Table 4
ANOVA table for lead removal using APTMS-Monosil

Source	Sum of squares (SS)	df	Mean square	F-Value	p-value
Model	18145.067	9	2016.118	77.143	< 0.0001
X_1	8206.843	1	8206.843	314.021	< 0.0001
X_2	3459.752	1	3459.752	132.381	< 0.0001
X_3	0.114	1	0.114	0.004	0.9486
X_1X_2	2947.968	1	2947.968	112.799	<0.0001
X_1X_3	7.430	1	7.430	0.284	0.6055
X_2X_3	6.319	1	6.319	0.242	0.6335
X_1^2	1109.030	1	1109.031	42.435	<0.0001
X_2^2	517.404	1	517.404	19.797	0.0012
X_3^2	5.989	1	5.989	0.229	0.6424
Residual	261.346	10	26.134		
Pure Error	0.00				
R^2					0.986
R^2_{adj}					0.973

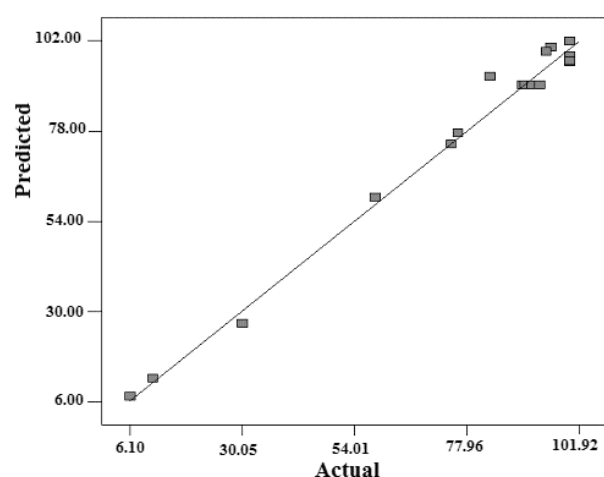


Fig. 3. Predicted versus experimental values plot for Pb^{2+} removal using APTMS-Monosil (predicted values: Eq. (3)).

the perturbation plot of Fig. 4. As expected from the analysis of the ANOVA table, Fig. 4 indicates that the effect of pH (X_1) on removal efficiency is quite strong, followed by the effect of solid to liquid ratio (X_2), with a weak dependence on Pb^{2+} initial concentration (X_3).

3.2.2. Response surface plots

Three-dimensional response surface plots were generated to further investigate the effects of the three process parameters considered, *i.e.* solution pH, solid to liquid ratio and initial concentration on Pb^{2+} removal.

3.2.3. Effect of pH

Figs. 5a and 5b show the effect of solution pH on the removal efficiency. According to these figures, the removal

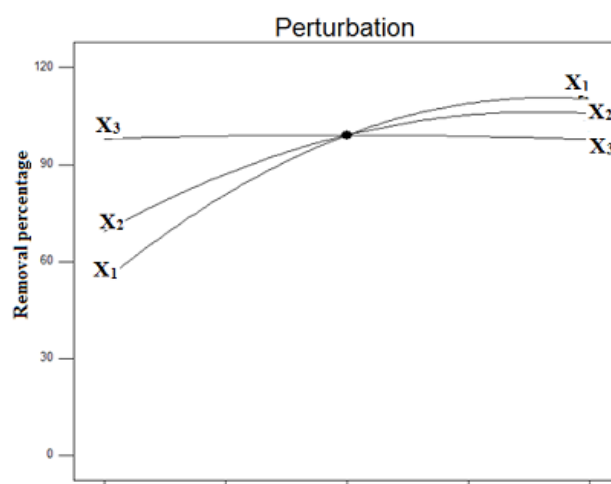


Fig. 4. Perturbation plot for Pb^{2+} removal at central point of design parameters. X_1 : pH; X_2 : solid to liquid ratio; X_3 : Pb^{2+} initial concentration. See Table 1 for the actual values of each parameter.

efficiency of Pb^{2+} increases with pH ranging from 2 to 6.5 at any fixed initial concentration and solid to liquid ratio, even though this effect is smaller when solid to liquid ratio increases. Presumably, the importance of solution pH in the removal process derives from its effect on the surface functional groups and the speciation of lead in solution. Indeed, the fact that pH_{ZPC} for APTMS-Monosil is 4.9 means that the surface charge of the adsorbent is positive when $pH < 4.9$ and negative when $pH > 4.9$. Since the dominant forms of lead at initial $pH < 6-6.5$ is Pb^{2+} cations [50,51], at $pH < pH_{ZPC}$ the surface of APTMS-Monosil is positively charged, and mainly an electrostatic repulsion occurs between Pb^{2+} cations and positive adsorption sites of APTMS-Monosil, while at $pH > pH_{ZPC}$, the adsorbent surface is negatively charged and it can more easily adsorb Pb^{2+} .

3.2.4. Effect of initial concentration

The effect of initial concentration is shown in Figs. 5b and 5c. The results indicate that this variable does not have a significant effect on removal efficiency regardless of pH and solid to liquid ratio, confirming the indications deriving from ANOVA table (p value = 0.9486).

3.2.5. Effect of solid to liquid ratio

According to Figs. 5a and 5c, the removal efficiency increases with increasing solid to liquid ratio. This tendency was expected because, as the ratio increases, so does the

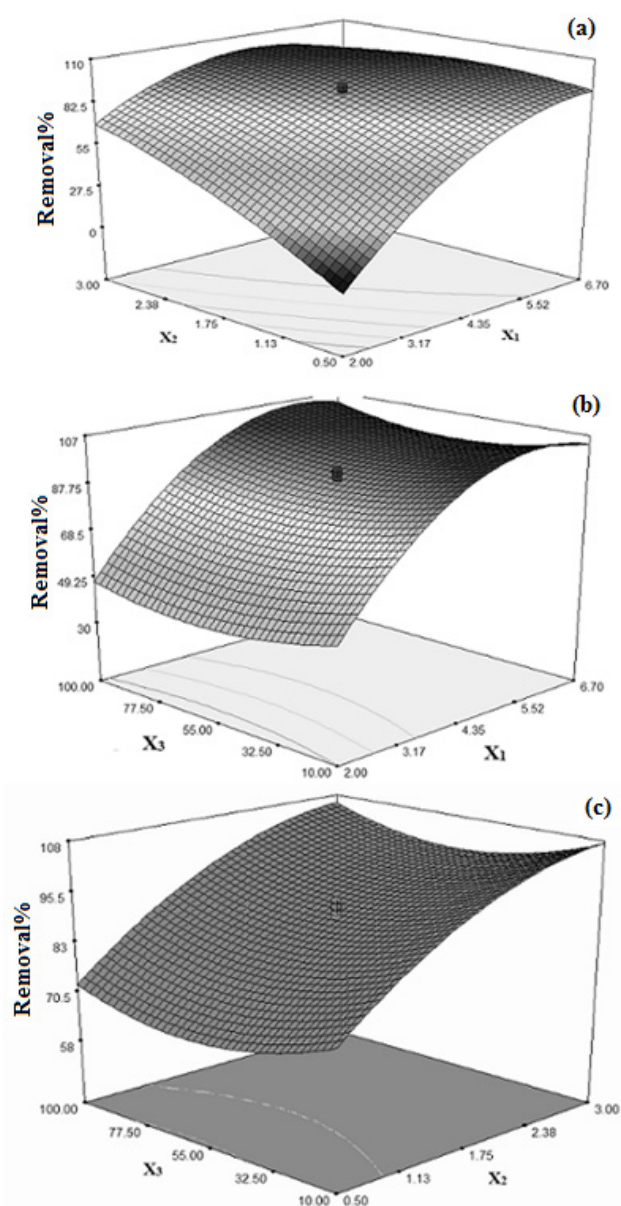


Fig. 5. Response surfaces plots for Pb²⁺ removal using APTMS-Monosil. (a): Effects of X₁ and X₂; (b): effects of X₁ and X₃; (c): effects of X₂ and X₃ (X₁: pH; X₂: solid to liquid ratio; X₃: Pb²⁺ initial concentration).

number of adsorbent active sites, and thus more Pb²⁺ ions can be removed.

Based on the optimum conditions, complete Pb²⁺ removal was predicted by the model under operating conditions of pH = 6.24, solid to liquid ratio 1.84 g L⁻¹ and initial concentration of 89.5 mg L⁻¹ for APTMS-Monosil. This result was validated experimentally (99.5% Pb²⁺ removal).

3.3. Adsorption kinetics

The adsorption kinetics were investigated in order to analyze the mechanism of adsorption and the potential rate controlling phenomena, such as mass transfer and chemical reaction. The adsorption kinetics of Pb²⁺ onto APTMS-Monosil were investigated by three common models, namely pseudo-first-order model, pseudo-second-order model and intraparticle diffusion model.

The pseudo-first-order model assumes that the limiting step of the adsorption process is the interaction between adsorbate molecules (here Pb²⁺ ions) and adsorbent active sites, and that this interaction can be kinetically described by a first order kinetic equation, with no role played by liquid–solid and intraparticle diffusion. If this model is appropriate, then the adsorption kinetics can be described by the following equation:

$$q_t = q_e (1 - e^{-k_1 t}) \quad (4)$$

where t (min) is time, q_e and q_t (mg g⁻¹) are the amount of Pb²⁺ adsorbed at equilibrium and at time t , respectively, and k_1 (min⁻¹) is the rate constant for the adsorption (pseudo) reaction.

The experimental data were also analyzed by the pseudo-second-order model, which once again assumes that the overall process is limited by the adsorbent–adsorbate interaction, but then assumes that this can be described by a second order kinetic equation. In this case the adsorption kinetics can be described by the following equation:

$$\frac{t}{q_t} = \frac{1}{k_2 q_e^2} + \frac{t}{q_e} \quad (5)$$

in which k_2 (g mg⁻¹ min⁻¹) is the rate constant for the adsorption (pseudo) reaction.

Eventually, the possibility that adsorption process is controlled by intraparticle diffusion was considered. If this is the case, then the adsorption kinetics can be described by the Morris–Weber model [52], according to which it is:

$$q_t = k_{id} t^{1/2} + \theta \quad (6)$$

in which k_{id} (mg·g⁻¹·min^{1/2}) is the intraparticle diffusion rate constant, and θ (mg g⁻¹) is a constant, the value of which depends on the role played by external (fluid–solid) mass transfer.

In order to compare the three models, the kinetic data relative to Pb²⁺ adsorption with solid to liquid ratio of 1 g·L⁻¹, initial Pb²⁺ concentration of 100 mg L⁻¹ and initial pH of 6.0 have been reported in Fig. 6. In particular, Fig. 6a refers to the pseudo-first-order model, and is a plot of $\ln(q_t)$ vs. t ;

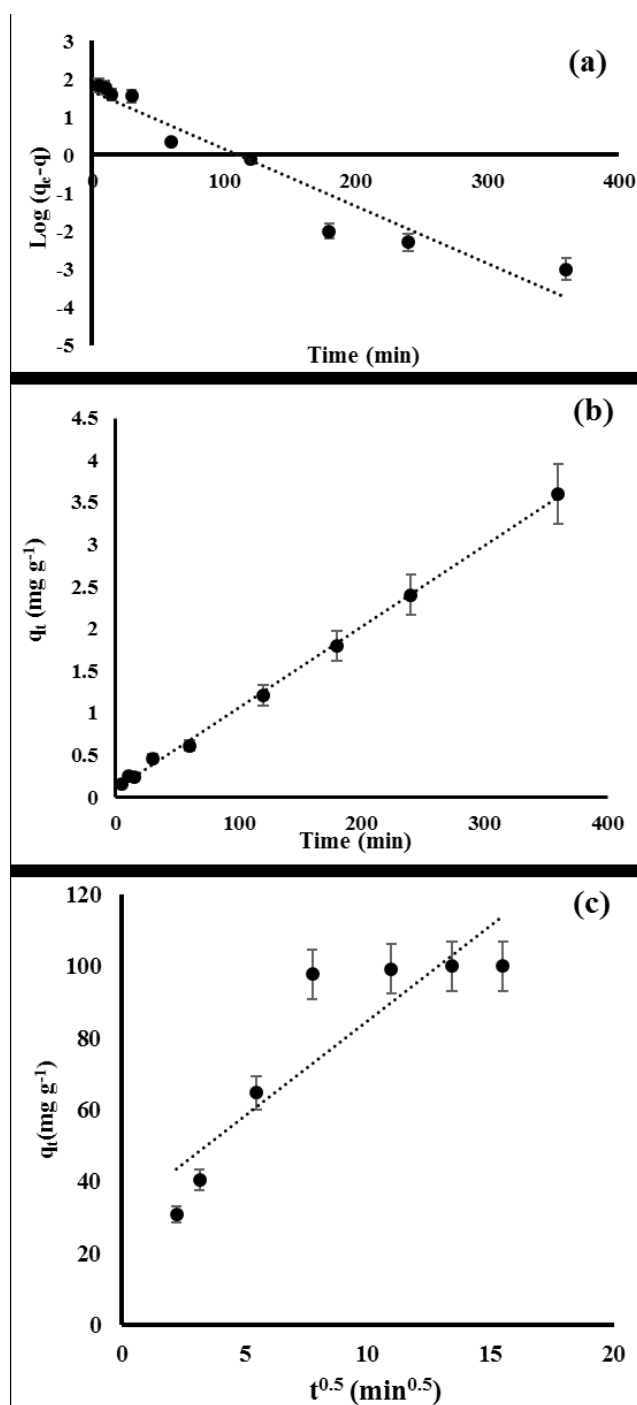


Fig. 6. (a) Pseudo-first-order model; (b) Pseudo-second-order model; (c) Intraparticle diffusion model for Pb²⁺ removal.

Fig. 6b refers to the pseudo-second-order model, and is a plot of $1/q_t$ vs. t ; eventually, Fig. 6c refers to the intraparticle diffusion model, and is a plot of q_t vs. $t^{1/2}$. Parameters and R^2 values for the three models are reported in Table 5. Inspection of Fig. 6 clearly indicates that experimental results are much better interpreted by the pseudo-second-order model than by the other models taken into account. This is also

confirmed by the fact that the R^2 value for the pseudo-second-order model is significantly closer to 1 than those relative to the two other models considered. This suggests that adsorption of Pb²⁺ on APTMS functionalised Monosil is controlled by a pseudo-chemical reaction, which can be described by a second order kinetic equation. In particular, the fact that the Weber–Morris model fails to describe the available kinetic data (see Fig. 6c) appears to indicate that intraparticle diffusion plays a secondary role in the overall adsorption process, at least in the experimental conditions considered.

3.4. Equilibrium and thermodynamic of adsorption

The equilibrium data relative to Pb²⁺ adsorption on APTMS-Monosil at 30°, 45° and 60°C are reported in Fig. 7. The most striking feature of Fig. 7 is that adsorption capacity increases with temperature, rather than decreasing, as is the case of most adsorption phenomena. In particular, the highest Pb²⁺ adsorption capacity, about 450 mg·g⁻¹, was observed at the highest temperature explored, *i.e.* $T = 60^\circ\text{C}$, with a behavior similar to the one exhibited by a number of amine-functionalized silicas toward gas-phase adsorption, in particular of CO₂ [27].

In order to have a clearer understanding of the adsorption process, the available data were fitted using the Langmuir, Freundlich and Dubinin–Raduskevich isotherms. The Langmuir isotherm is based on the assumptions that all the adsorption sites are equivalent for what concerns adsorbent–adsorbate interactions, that each site only interacts with a single adsorbate molecule/ion and that adsorbate–adsorbate interactions are negligible. The Langmuir isotherm equation is described by the following equation:

$$q_e = q_{\max} \frac{K_L C_e}{1 + K_L C_e} \quad (7)$$

where C_e (mg g⁻¹) is the liquid phase concentration of adsorbate at equilibrium and K_L (L·mg⁻¹) and q_{\max} (mg·g⁻¹) are the model parameters: q_{\max} represents the maximum amount of adsorbate which can be theoretically adsorbed per unit mass of adsorbent when the monolayer coverage is complete, while K_L is a measure of adsorbent–adsorbate affinity.

The Freundlich isotherm is an essentially empirical equation, which assumes that the adsorption process takes place on a heterogeneous surface, and is described by the following equation:

$$q_e = K_f (C_e)^{1/n} \quad (8)$$

where K_f and n are the model parameters: K_f (mg g⁻¹ L^{1/n} mg^{-1/n}) is an indicator of the adsorption capacity of adsorbent and n is a measure of favorability of adsorption.

The Dubinin–Radushkevich (D-R) isotherm is a model originally proposed to describe gas-phase adsorption of subcritical vapors on porous sorbents, and can in general be used to describe adsorption on a heterogeneous surface characterized by a Gaussian distribution of adsorbent–adsorbate interaction energy [53]. The D–R equation is described by Eq. (9):

Table 5
Constants and regression coefficient for kinetic models

Pseudo-first-order			Pseudo-second-order			Intra-particle diffusion		
k_1 (min ⁻¹)	q_e (mg g ⁻¹)	R^2	k_2 (g mg ⁻¹ .min ⁻¹)	q_e (mg g ⁻¹)	R^2	k_{id} (mg g ⁻¹ .min ^{-1/2})	θ	R^2
0.034	46.54	0.92	0.0009	104.16	0.998	5.32	31.63	0.778

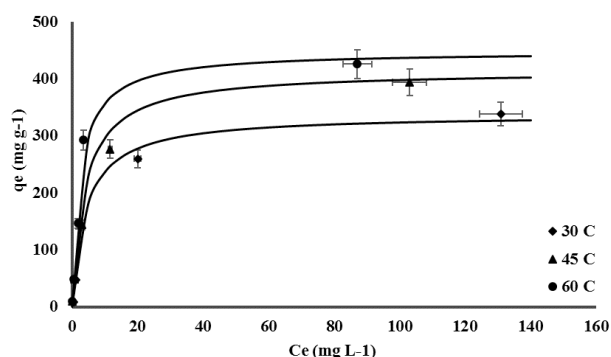


Fig. 7. Adsorption isotherms of Pb²⁺ on APTMS-Monosil $T = 30^\circ$, 45° and 60°C (points: experimental data; continuous curves: Langmuir isotherms with parameters taken from Table 6).

$$\begin{cases} q_e = q_{\max} \exp\left[-\frac{1}{2}\left(\frac{\varepsilon}{E}\right)^2\right] \\ \varepsilon = RT \ln\left(1 + \frac{1}{C_e}\right) \end{cases} \quad (9)$$

where R and T are the gas constant ($\text{kJ mol}^{-1} \text{K}^{-1}$) and absolute temperature (K), respectively, and q_{\max} ($\text{mg}\cdot\text{g}^{-1}$) and E (kJ mol^{-1}) are the model parameters. As indicated above, q_{\max} represents the maximum possible amount of adsorbate; E , on the other hand, is the mean free energy of adsorption per mole of adsorbate when it is transferred to the surface of solid from infinity in the solution.

In order to compare the three isotherms considered, the optimal values of the parameters were estimated starting from the linearized forms of Eqs. (7–9). The results of the regressions, together with the regression coefficients R^2 , are presented in Table 6. The comparison among the different regressions indicates that the Langmuir isotherm consistently gives the best fit to experimental data, and for this reason the curves relative to the Langmuir isotherms using the parameters taken from Table 6 have been reported in Fig. 7.

The results of Table 6 and the very good agreement between Langmuir isotherms and experimental data shown in Fig. 7 suggest that Pb²⁺ adsorption on APTMS-Monosil takes place as a monolayer or, in other words, that all the adsorbing sites are equivalent, and capable of capturing a single Pb²⁺ ion each. In particular, the amino groups available on the silica surface can form complexes with Pb²⁺ ions [13], and it can be assumed that each couple of amino groups adsorbs a Pb²⁺ ion according to the scheme of Fig. 8.

Table 6
Langmuir, Freundlich and D-R isotherm constant parameters.

Isotherm	Parameters	30°C	45°C	60°C
Langmuir	q_{\max} (mg g ⁻¹)	337.3	413.6	448.1
	K_L (L mg ⁻¹)	0.232	0.248	0.383
	R^2	0.964	0.981	0.973
Freundlich	K_f (mg g ⁻¹ L ^{1/n} mg ^{1/n})	85.81	101.17	130.33
	n (-)	3.396	3.286	3.636
	R^2	0.874	0.926	0.840
D-R	E (kJ mol ⁻¹)	0.543	0.459	0.743
	q_{\max} (mol g ⁻¹)	313.1	364.0	423.3
	R^2	0.828	0.918	0.964

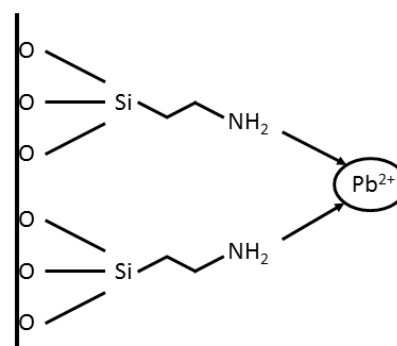


Fig. 8. Schematic of adsorption mechanism of Pb²⁺ by APTMS-Monosil nanocomposite.

Furthermore, it is interesting to observe that both the maximum adsorption capacity q_{\max} and the affinity constant K_L significantly increase with temperature: q_{\max} has an almost fivefold increase between 30°C and 60°C: this could be due to a more active chelating effect of amino groups with increasing temperature. For what concerns K_L , its dependence on temperature was used to determine the thermodynamic parameters of the adsorption process according to the following equations:

$$\begin{cases} \Delta G^\circ = -RT \ln K_L \\ \ln K_L = \frac{-\Delta H^\circ}{RT} + \frac{\Delta S^\circ}{R} \\ T\Delta S^\circ = \Delta H^\circ - \Delta G^\circ \end{cases} \quad (10)$$

where ΔG° , ΔH° and ΔS° are the standard changes in Gibbs free energy, enthalpy and entropy, respectively. ΔH° and ΔS°

can be obtained as the slope and intercept of a plot of $\ln(K_L)$ vs. $1/T$ (Fig. 9). Calculated thermodynamic parameters are reported in Table 7.

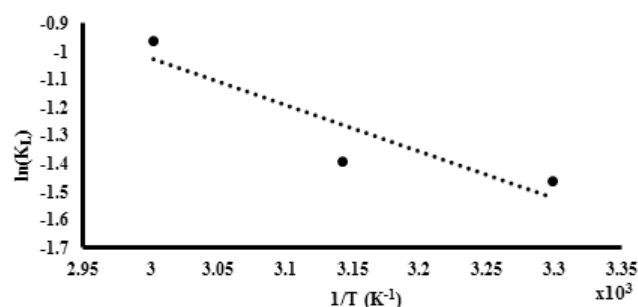


Fig. 9. Relationship between $\ln(K_L)$ and $1/T$ for Pb^{2+} adsorption on APTMS-Monosil.

Table 7
Thermodynamic parameters at $T = 298$ K for Pb^{2+} adsorption on APTMS-Monosil

ΔH° , $\text{kJ}\cdot\text{mol}^{-1}$	30.9
DS° , $\text{kJ}\cdot\text{mol}^{-1}\text{K}^{-1}$	0.187
ΔG° , $\text{kJ}\cdot\text{mol}^{-1}$	-24.826

Table 8
Comparison of Pb^{2+} adsorption capacity (mg g^{-1}) of different adsorbents [45,46,49–62]

Adsorbent	Pb^{2+} adsorption capacity (mg g^{-1})	Reference
Goethite nanoparticles	820.5	49
HAp/ Fe_3O_4 microspheres	540	62
Modified mesoporous carbon	500	50
APTMS-Monosil	450	(This work)
Chitosan nanoparticles	400	51
Hydrated maganes oxide (HMO)	325	52
Polymer-based hybrid	181.4	53
Zeolite (Clinoptilolite)-pretreated	122	58
Iron-activated carbon (IAC) nanocomposite	121.9	61
MHC/OMCNTs	116.3	54
$\text{Co}_{0.6}\text{Fe}_{2.4}\text{O}_4$ micro-particles	80.32	59
Activated carbon/ Fe_3O_4 nanocomposite	71.42	60
Activated carbon	51.81	46
Pine cone activated carbon	27.53	45
Fe_3O_4 nanospheres	18.47	55
$\text{Fe}_3\text{O}_4/\text{SiO}_2$ nanocomposite	17.65	56
Nanometer titanium dioxide/silica gel	3.16	57

The positive value of ΔH° confirms that the Pb^{2+} adsorption on APTMS-Monosil has an endothermic nature. Furthermore, its relatively high value is in good agreement with the adsorption mechanism devised above, which has a strong chemical (rather than purely physical) nature. Eventually, it must be pointed out that the high value of DS° counterbalances the value of ΔH° , leading to a negative ΔG° (spontaneous process).

The maximum adsorption capacity of APTMS-Monosil for Pb^{2+} (about $450 \text{ mg}\cdot\text{g}^{-1}$ at $T = 60^\circ\text{C}$.) was also compared with the adsorption capacity of other adsorbents proposed for Pb^{2+} removal [50,51,54–67]. The results of this comparison, reported in Fig. 10 and in Table 8, indicate that APTMS-Monosil has very interesting performances.

3.5. Regenerability tests

In order to verify the capacity of APTMS-Monosil to withstand a number of repeated adsorption–desorption cycles, a series of experiments in which the same sample was used to remove Pb^{2+} from a solution having a Pb^{2+} concentration of 100 mg/l was carried out. As mentioned above, between two removal experiments the sample was regenerated by treatment with 0.1 M EDTA . The results for adsorption–desorption cycles of Pb^{2+} are presented in Fig. 11. As the results show, the adsorption percentage of lead decreased from

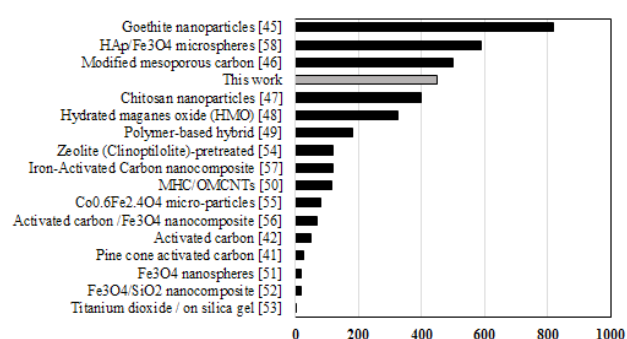


Fig. 10. Comparison of Pb^{2+} adsorption capacity (mg g^{-1}) of different adsorbents [45,46,49–62].

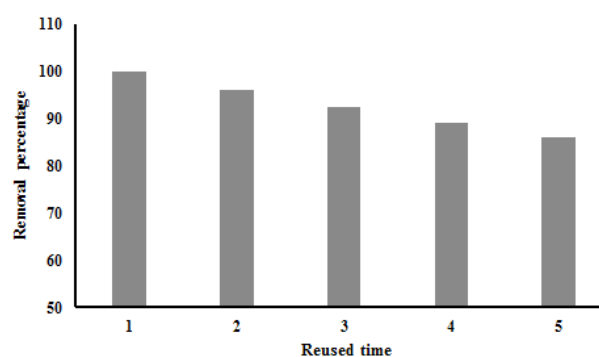


Fig.11. Removal efficiency of Pb^{2+} on APTMS-Monosil as a function of regeneration cycles of the adsorbent.

100% to 86.4%. The limited extent of decrease in adsorption indicates a very high regenerability of the proposed material.

4. Conclusions

Amino-functionalized silica monolith (APTMS-Monosil) was synthesized and tested in several batch experiments as a highly porous adsorbent for Pb²⁺ removal from aqueous solution. The RSM results indicated that solution pH and solid to liquid ratio are the most significant removal parameters, and that the optimum operating conditions are pH of 5.9, solid to liquid ratio of 1.74 g L⁻¹ and initial Pb²⁺ concentration of 84 mg L⁻¹. In these conditions, practically 100% of Pb²⁺ present in solution can be removed by APTMS-Monosil. The kinetics of Pb²⁺ removal is controlled by the adsorption pseudo-reaction rather than intraparticle diffusion, and this reaction can be described by a second order kinetic equation. The Langmuir isotherm satisfactorily describes equilibrium adsorption of Pb²⁺ on APTMS-Monosil. Results show that this process has a markedly chemical nature, and that the maximum adsorption capacity of APTMS-Monosil is about 450 mg·g⁻¹ at 60°C. The comparison between the adsorption capacity exhibited by APTMS-Monosil and the capacities reported in the literature for other adsorbing materials is very favorable. Furthermore, APTMS-Monosil exhibits a good capacity of withstanding several adsorption-regeneration cycles.

Based on this analysis, APTM-functionalized Monosil adsorbent could be an excellent candidate for practical applications in the removal of Pb²⁺ from wastewater, and continuous removal experiments in columns systems should be carried out in order to better evaluate it. Last but by now way least, preparation and application costs of APTMS-Monosil will have to be taken into account to fully ascertain its practical applicability.

References

- [1] K.K. Wong, C.K. Lee, K.S. Low, M.J. Haron, Removal of Cu(II) and Pb(II) by tartaric acid modified rice husk from aqueous solutions, *Chemosphere*, 50 (2003) 23–28.
- [2] R. Jalali, H. Ghafourian, Y. Asef, S.J. Davarpanah, S. Sepehr, Removal and recovery of lead using nonliving biomass of marine algae, *J. Hazard. Mater.*, 92 (2002) 253–262.
- [3] V.K. Gupta, M. Gupta, S. Sharma, Process development for the removal of lead and chromium from aqueous solutions using red mud—an aluminum industry waste, *Water Res.*, 35 (2001) 1125–1134.
- [4] K. Conrad, H.C.B. Hansen, Sorption of zinc and lead on coir, *Bioresour. Technol.*, 98 (2007) 89–97.
- [5] T. Bahadir, G. Bakan, L. Altas, H. Buyukgungor, the investigation of lead removal by biosorption: an application at storage battery industry wastewaters, *Enzyme Microb. Technol.*, 41 (2007) 98–102.
- [6] R. Brooks, M. Bahadory, F. Tovia, H. Rostami, Removal of lead from contaminated water, *Int. J. Soil Sedim. Water*, 3 (2010) 1–13.
- [7] K. Li, Z. Zheng, Y. Li, J. Characterization and lead adsorption properties of activated carbons prepared from cotton stalk by one-step H₃PO₄ activation, *J. Hazard. Mater.*, 181 (2010) 440–447.
- [8] F. Pepe, B. de Gennaro, P. Aprea, D. Caputo, Natural zeolites for heavy metals removal from aqueous solutions: Modeling of the fixed bed Ba²⁺/Na⁺ ion-exchange process using a mixed phillipsite/chabazite-rich tuff, *Chem. Eng. J.*, 219 (2013) 37–42.
- [9] E. Pehlivan, T. Altun, Ion-exchange of Pb²⁺, Cu²⁺, Zn²⁺, Cd²⁺, and Ni²⁺ ions from aqueous solution by Lewatit CNP 80, *J. Hazard. Mater.*, 140 (2007) 299–307.
- [10] S. Vasudevan, J. Lakshmi, G. Sozhan, Effects of alternating and direct current in electrocoagulation process on the removal of cadmium from water, *J. Hazard. Mater.*, 192 (2011) 26–34.
- [11] S. Zhang, F. Xu, Y. Wang, W. Zhang, X. Peng, F. Pepe, Silica modified calcium alginate-xanthan gum hybrid bead composites for the removal and recovery of Pb(II) from aqueous solution, *Chem. Eng. J.*, 234, (2013) 33–42.
- [12] S. Hydari, H. Sharififard, M. Nabavinia, M.R.A Parvizi, Comparative investigation on removal performances of commercial activated carbon, chitosan biosorbent and chitosan/activated carbon composite for cadmium, *Chem. Eng. J.*, 193 (2012) 276–282.
- [13] S. Hao, Y. Zhong, F. Pepe, W. Zhu, Adsorption of Pb²⁺ and Cu²⁺ on anionic surfactant-templated amino-functionalized mesoporous silicas, *Chem. Eng. J.*, 189–190 (2012) 160–167.
- [14] V.K. Gupta, I. Ali, T.A. Saleh, A. Nayak, S. Agarwal, Chemical treatment technologies for waste-water recycling—an overview, *Rsc Advances*, 2 (2012) 6380–6388.
- [15] H. Sharififard, F. Zokaee Ashtiani, M. Soleimani, Adsorption of palladium and platinum from aqueous solutions by chitosan and activated carbon coated with chitosan, *Asia-Pac. J. Chem. Eng.*, 8 (2013) 384–395.
- [16] V. K. Gupta, A. Nayak, S. Agarwal, Bioadsorbents for remediation of heavy metals: current status and their future prospects, *Environ. Eng. Res.*, 20 (2015) 1–18.
- [17] V.K. Gupta, S. Agarwal, T.A. Saleh, Synthesis and characterization of alumina-coated carbon nanotubes and their application for lead removal, *J. Hazard. Mat.*, 185 (2011) 17–23.
- [18] H. Sharififard, M. Soleimani, F. Zokaee Ashtiani, Evaluation of activated carbon and bio-polymer modified activated carbon performance for palladium and platinum removal, *J. Taiwan Inst. Chem Eng.*, 43 (2012) 696–703.
- [19] N. Mehrabi, M. Soleimani, M. Madadi Yeganeh, H. Sharififard, Parameters optimization for nitrate removal from water using activated carbon and composite of activated carbon and Fe₃O₄ nanoparticles, *RSC Adv.*, 5 (2015) 51470–51482.
- [20] S.U. Khan, I.H. Farooqi, S. Ayub, Studies on application of Fe based binary oxide nanoparticles for treatment of lead (Pb²⁺) contaminated water - A batch study, *Mater. Today: Proc.*, 4 (2017) 9650–9655.
- [21] S. Rajput, C.U. Pittman, D. Mohan, Magnetic magnetite (Fe₃O₄) nanoparticle synthesis and applications for lead (Pb²⁺) and chromium (Cr⁶⁺) removal from water, *J. Colloid Interface Sci.*, 468 (2016) 334–346.
- [22] M. Liu, Y. Wang, L. Chen, Y. Zhang, Z. Lin, Mg(OH)₂ Supported nanoscale zero valent iron enhancing the removal of Pb(II) from aqueous solution, *ACS Appl. Mater. Interf.*, 7 (2015) 7961–7969.
- [23] A. Gil, M.J. Amiri, J. Abedi-Koupai, S. Eslamian, Adsorption/reduction of Hg(II) and Pb(II) from aqueous solutions by using bone ash/nZVI composite: effects of aging time, Fe loading quantity and co-existing ions, *Environ. Sci. Pollut. Res. Int.*, (2017) 1–16.
- [24] M.J. Amiri, J. Abedi-Koupai, S.S. Eslamian, M. Arshadi, Adsorption of Pb(II) and Hg(II) ions from aqueous single metal solutions by using surfactant-modified ostrich bone waste, *Desal. Water Treat.*, 57 (2016) 1–18.
- [25] M. Bhatia, S.B. Rajulapati, S. Sonawane, A. Girdhar, Synthesis and implication of novel poly(acrylic acid)/nanosorbent embedded hydrogel composite for lead ion removal, *Scientific Reports*, 7 (2017) 1–16.
- [26] B. Levasseur, A.M. Ebrahim, T.J. Bandosz, Interactions of NO₂ with amine-functionalized SBA-15: effects of synthesis route, *Langmuir*, 28 (2012) 5703–5714.
- [27] N. Gargiulo, A. Peluso, P. Aprea, F. Pepe, D. Caputo, CO₂ Adsorption on polyethylenimine-functionalized SBA-15 mesoporous silica: isotherms and modeling, *J. Chem. Eng. Data*, 59 (2014) 896–902.
- [28] V. Manu, M.M. Hareesh, C.B. Hari, V.J. Raksh, Adsorption of Cu²⁺ on amino functionalized silica gel with different loading, *Ind. Eng. Chem. Res.*, 48 (2009) 8954–8960.

- [29] J.S. Li, X.Y. Miao, Y.X. Hao, J.Y. Zhao, X.Y. Sun, L.J. Wang, Synthesis, amino-functionalization of mesoporous silica and its adsorption of Cr(VI), *J. Colloid Interf. Sci.*, 318 (2008) 309–314.
- [30] M.V. Lombardo, M. Videla, A. Calvo, F.G. Requejo, G.J.A.A. Soler-Illi, Aminopropyl-modified mesoporous silica SBA-15 as recovery agents of Cu(II)-sulfate solutions: adsorption efficiency, functional stability and reusability aspects, *J. Hazard. Mater.*, 223–224 (2012) 53–62.
- [31] S. Hao, A. Verlotto, P. Aprea, F. Pepe, D. Caputo, W. Zhu, Optimal synthesis of amino-functionalized mesoporous silicas for the adsorption of heavy metal ions, *Microp. Mesop. Mater.*, 236 (2016) 250–259.
- [32] A. Sachse, A. Galarneau, F. Fajula, F. Di Renzo, P. Creux, B. Coq, Functional silica monoliths with hierarchical uniform porosity as continuous flow catalytic reactors, *Microp. Mesop. Mater.*, 140 (2011) 58–68.
- [33] K. Nakanishi, N. Soga, Phase separation in gelling silica-organic polymer solution: systems containing poly(sodium styrenesulfonate), *J. Am. Cer. Soc.*, 74 (1991) 2518–2530.
- [34] A. Inayat, B. Reinhardt, H. Uhlig, W. Einicke, D. Enke, Silica monoliths with hierarchical porosity obtained from porous glasses, *Chem. Soc. Rev.*, 42 (2013) 3753–3764.
- [35] N. Gargiulo, A. Verlotto, A. Peluso, P. Aprea, D. Caputo, Modeling the performances of a CO₂ adsorbent based on polyethyleneimine-functionalized macro-mesoporous silica monoliths, *Microp. Mesop. Mater.*, 215 (2015) 1–7.
- [36] E. Sugrue, P. Nesterenko, B. Paull, Ion exchange properties of monolithic and particle type iminodiacetic acid modified silica, *J. Sep. Sci.*, 27 (2004) 921–930.
- [37] M.R. Awual, T. Yaita, S.A. El-Safty, H. Shiwaku, S. Suzuki, Y. Okamoto, Copper(II) ions capturing from water using ligand modified a new type mesoporous adsorbent, *Chem. Eng. J.*, 221 (2013) 322–330.
- [38] M.R. Awual, M. Ismael, T. Yaita, Efficient detection and extraction of cobalt(II) from lithium ion batteries and wastewater by novel composite adsorbent, *Sensors Actuators B: Chem.*, 191 (2014) 9–18.
- [39] R. Azargohar, A.K. Dalai, Production of activated carbon from Luscar char: experimental and modelling studies, *Micropor. Mesop. Mat.*, 85 (2005) 219–225.
- [40] M. Jain, V.K. Garg, K. Kadirvelu, Investigation of Cr(VI) adsorption onto chemically treated *Helianthus annuus*: optimization using response surface methodology, *Bioresour. Technol.*, 102 (2011) 600–605.
- [41] D.C. Montgomery, *Design and Analysis of Experiments*, 5th ed., John Wiley & Sons, New York, 2001.
- [42] R.H. Myers, D.C. Montgomery, *Response Surface Methodology: Process and Product Optimization Using Designed Experiments*, 2nd ed., John Wiley & Sons, New York, 2002.
- [43] M. Roso, A. Lorenzetti, S. Besco, M. Monti, G. Berti, M. Modesti, Application of empirical modelling in multi-layers membrane manufacturing, *Comp. Chem. Eng.*, 35 (2011) 2248–2256.
- [44] E. Da'na, A. Sayari, Adsorption of copper on amine-functionalized SBA-15 prepared by co-condensation: equilibrium properties, *Chem. Eng. J.*, 166 (2011) 445–453.
- [45] S. Lowell, J.E. Shields, M.A. Thomas, M. Thommes, *Characterization of Porous Materials and Powders: Surface Area, Pore Size and Density*, Springer, Dordrecht, 2004.
- [46] F.N. Aarden, *Adsorption onto Heterogeneous Porous Materials: Equilibria and Kinetics*. Ph.D. Dissertation, Technische Universiteit Delft, 2001.
- [47] H. Sanaeishoar, M. Sabbaghan, F. Mohave, Synthesis and characterization of micro-mesoporous MCM-41 using various ionic liquids as co-templates, *Micropor. Mesop. Mater.*, 217 (2015) 219–224.
- [48] R.A. Fischer, *Statistical Methods for Research Worker*, Oliver & Boyd, London, 1925.
- [49] K.Y. Nandiwale, N.D. Galande, V.V. Bokade, Process optimization by response surface methodology for transesterification of renewable ethyl acetate to butyl acetate biofuel additive over borated USY zeolite, *RSC Adv.*, 5 (2015) 17109–17116.
- [50] M. Momcilovic, M. Purenov, A. Zarubica, M. Randelovic, Removal of lead(II) ions from aqueous solutions by adsorption onto pine cone activated carbon, *Desalination*, 276 (2011) 53–59.
- [51] S.Z. Mohammadi, M.A. Karimi, D. Afzali, F. Mansouri, Removal of Pb(II) from aqueous solutions using activated carbon from sea-buckthorn stones by chemical activation, *Desalination*, 262 (2010) 86–93.
- [52] B.H. Hameed, A.A. Ahmad, Batch adsorption of Methylene blue aqueous solution by garlic peel, an agricultural waste biomass, *J. Hazard. Mater.*, 164 (2009) 870–875.
- [53] K.Y. Foo, B.H. Hameed, Insights into the modeling of adsorption isotherm systems, *Chem. Eng. J.*, 156 (2010) 2–10.
- [54] S. Rahimi, R.M. Moattari, L. Rajabi, A.A. Derakhshan, M. Keyhani, Iron oxide/hydroxide (α,γ -FeOOH) nanoparticles as high potential adsorbents for lead removal from polluted aquatic media, *J. Ind. Eng. Chem.*, 23 (2015) 33–43.
- [55] G. Zolfaghari, A. Esmaili-Sari, M. Anbia, H. Younesi, S. Amirmahmoodi, A. Ghafari-Nazari, Taguchi optimization approach for Pb(II) and Hg(II) removal from aqueous solutions using modified mesoporous carbon, *J. Hazard. Mater.*, 192 (2011) 1046–1055.
- [56] L. Qi, Z. Xu, Lead sorption from aqueous solutions on chitosan nanoparticles, *Colloid Surf. A*, 251 (2004) 183–190.
- [57] Q. Su, B. Pan, Q. Zhang, W. Zhang, L. Lv, X. Wang, J. Wu, Q. Zhang, Fabrication of polymer-supported nanosized hydrous manganese dioxide (HMO) for enhanced lead removal from waters, *Sci. Total. Environ.*, 407 (2009) 5471–5477.
- [58] V. Vetriselvi, R. Jaya Santhi, Redox polymer as an adsorbent for the removal of chromium (VI) and lead (II) from the tannery effluents, *Water Resour. Ind.*, 10 (2015) 39–52.
- [59] Y. Wang, L. Shi, L. Gao, Q. Wei, L. Cui, L. Hu, L. Yan, B. Du, The removal of lead ions from aqueous solution by using magnetic hydroxypropyl chitosan/oxidized multiwalled carbon nanotubes, *J. Colloid Interf. Sci.*, 451 (2015) 7–14.
- [60] M. Kumari, C.U. Pittman Jr, D. Mohan, Heavy metals [chromium (VI) and lead (II)] removal from water using mesoporous magnetite (Fe₃O₄) nanospheres, *J. Colloid Interf. Sci.*, 442 (2015) 120–132.
- [61] M. Mahdavi, M.B. Ahmad, M.J. Haron, Y. Gharayebi, K. Shamel, B. Nadi, Fabrication and characterization of SiO₂/(3-aminopropyl) triethoxysilane-coated magnetite nanoparticles for lead(II) removal from aqueous solution, *J. Inorg. Organomet. Polym.*, 23 (2013) 599–607.
- [62] R. Lui, P. Liang, Determination of trace lead in water samples by graphite furnace atomic absorption spectrometry after preconcentration with nanometer titanium dioxide immobilized on silica gel, *J. Hazard. Mater.*, 152 (2008) 166–171.
- [63] A. Gunay, E. Arslankaya, I. Tosun, Lead removal from aqueous solution by natural and pretreated clinoptilolite: adsorption equilibrium and kinetics, *J. Hazard. Mater.*, 146 (2007) 362–371.
- [64] D. Shengxia, T. Rongfeng, X. Zechun, Z. Xianxi, Z. Yueying, Z. Wen, Z. Junhong, W. Bingquan, Z. Suyuan, S. Dezhi, Effective removal of Pb(II) using magnetic Co_{0.6}Fe_{2.4}O₄ micro-particles as the adsorbent: synthesis and study on the kinetic and thermodynamic behaviors for its adsorption, *Colloids Surf. A*, 469 (2015) 211–223.
- [65] B. Kakavandi, R. Rezaei Kalantary, A. Jonidi Jafari, S. Nasser, A. Ameri, A. Esrafil, A. Azari, Pb(II) adsorption onto a magnetic composite of activated carbon and superparamagnetic Fe₃O₄ nanoparticles: experimental and modeling study, *Clean—Soil Air Water*, 43 (2015) 1157–1166.
- [66] H. Sharififard, F. Pepe, M. Soleimani, P. Aprea, D. Caputo, Iron-activated carbon nanocomposite: synthesis, characterization and application for lead removal from aqueous solution, *RSC Adv.*, 6 (2016) 42845–42853.
- [67] Z. Fuqiang, T. Ruiqin Tan, S. Wenfeng, Z. Xianpeng, X. Wei, S. Weijie, Monodisperse magnetic hydroxyapatite/Fe₃O₄ microspheres for removal of lead(II) from aqueous solution, *J. Alloys Comp.*, 637 (2015) 531–537.